

Electronic Supplementary Information

From waste carbonated beverages to high performance electrochromic devices: a green and low-cost synthetic method for self-doped metal oxides

Lingqi Wu, Huajing Fang,* Kai Jing, Haolin Yu and Zhiwei Shan

Center for Advancing Materials Performance from the Nanoscale (CAMP-Nano), State Key Laboratory for Mechanical Behavior of Materials, Xi'an Jiaotong University, Xi'an 710049, China

*E-mail: fanghj@xjtu.edu.cn

The details of carbonated beverage ingredients:

Cola: Water, fructose syrup, sugar, food additives (carbon dioxide, caramel color, phosphoric acid, caffeine, food flavor).

Sprite: Water, fructose syrup, sugar, food flavorings, food additives (carbon dioxide, citric acid, sodium citrate, sodium benzoate).

Fanta: Water, fructose syrup, sugar, food flavorings (carbon dioxide, citric acid, sodium benzoate, sodium hexametaphosphate, stevia glycoside, lemon yellow, brilliant blue).

The detailed steps of the preparation procedure for pure WO₃:

3 g AMT powder was added to 27 g deionized water and then stirred for 30 min until completely dissolved to obtain a dark brown tungsten oxide precursor. The precursor was aged for 24 h before use. The conductive fluorine-doped tin oxide (FTO) glasses were ultrasonically cleaned with acetone, ethanol, and deionized water for 15 min, respectively. Air plasma treatment was applied for hydrophilic improvement of the FTO glass subsequently. Then, the precursor was spin-coated on the cleaned FTO glass at 1800 rpm for 8 s and dried at 300 °C for 5 min. Spin-coating step was repeated six times to reach the proper thickness. Next, the spin-coated sample was transferred to a 350 °C hot plate for 30 min. Finally, the thin film was annealed at 450 °C for 2 h in a muffle furnace to obtain the WO₃ thin film.



Fig. S1 The digital photographs of the colloidal precursor after being left for different periods of time.

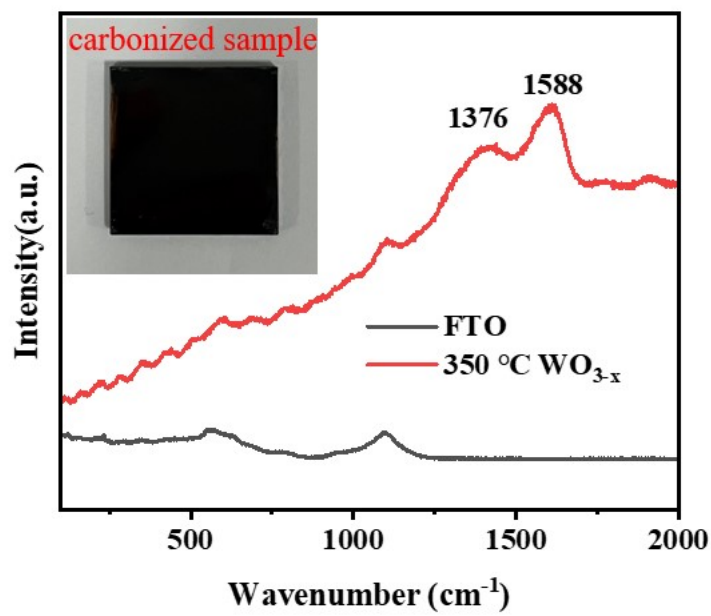


Fig. S2 Raman spectra of the FTO substrate and the carbonized sample, inset is a photograph of the carbonized sample at 350 °C.

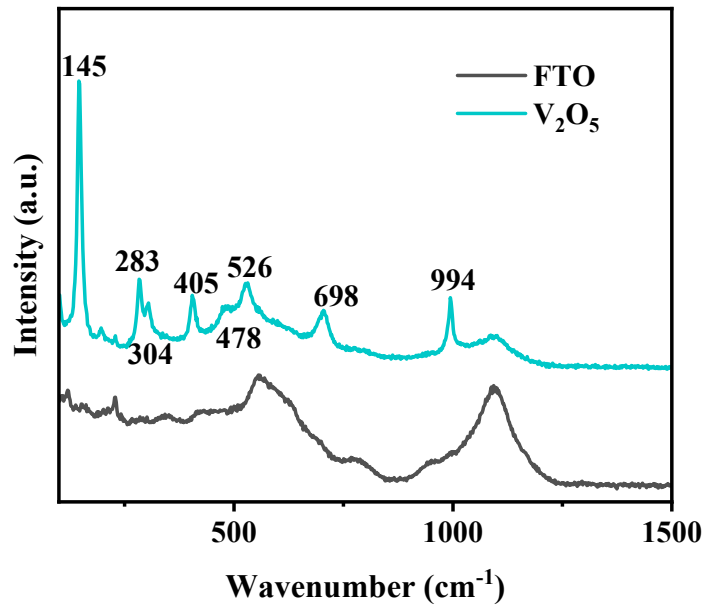


Fig. S3 Raman spectra of the FTO substrate and the annealed V₂O₅ film.

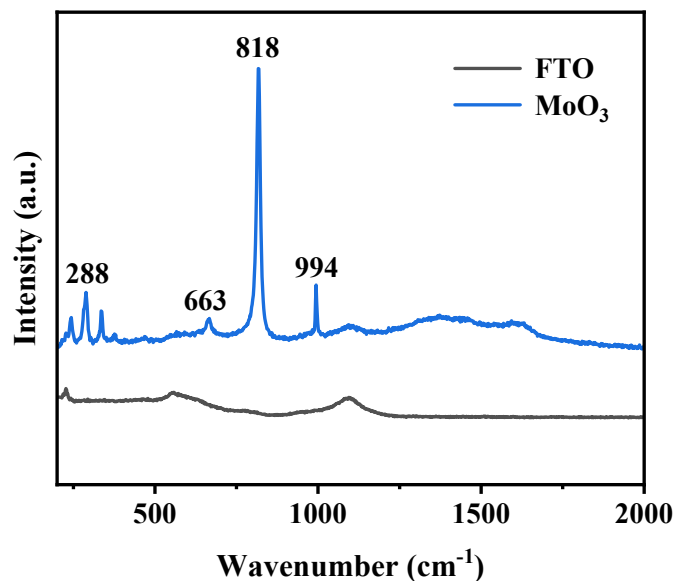


Fig. S4 Raman spectra of the FTO substrate and the annealed MoO₃ film.

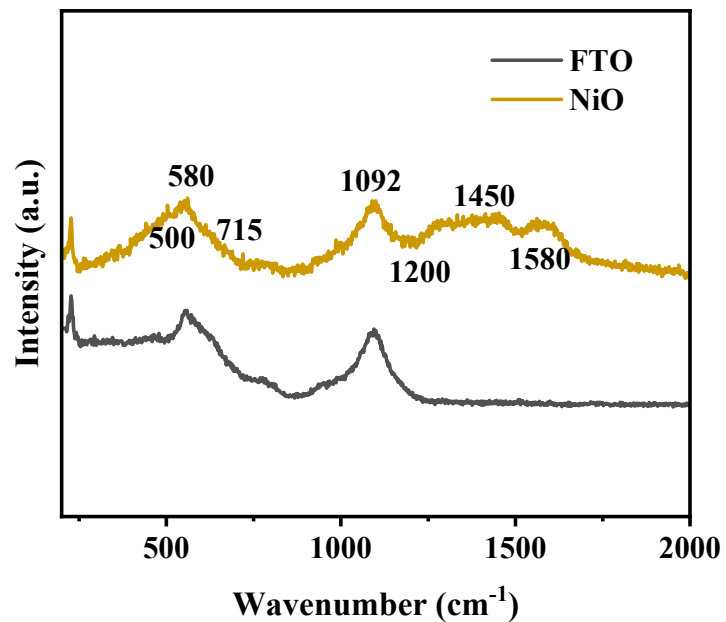
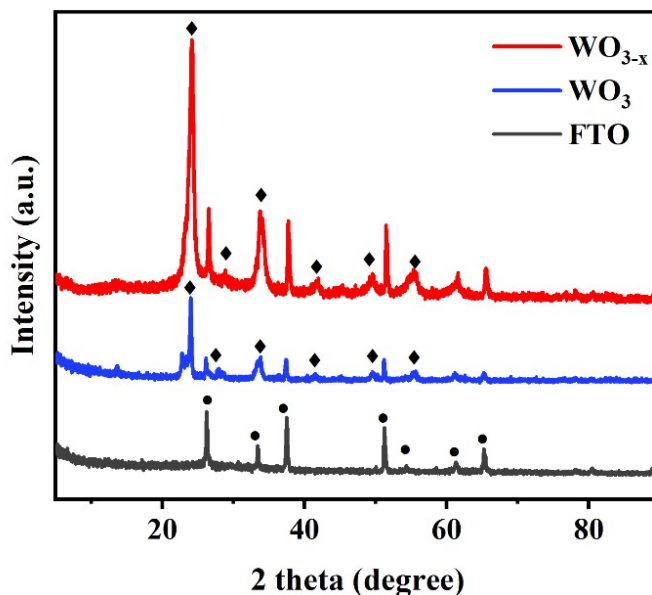


Fig. S5 Raman spectra of the FTO substrate and the annealed NiO film.

The characteristic peaks at 145 (lattice vibration), 283 (V=O bending), 304 (V-O bending vibration), 405 (V=O bending vibration), 478 (V-O-V stretching), 526, 698 (doubly coordinated oxygen bonds) and 994 (V=O terminal bonding) cm^{-1} verify the formation of vanadium pentoxide (Fig. S2). The typical fingerprint vibration modes at 288 (O=M=O), 663 (3Mo-O), 813(2Mo-O), and 994 (Mo^{6+} -O) cm^{-1} are observed on the molybdenum oxide (Fig. S3). And the peaks of 500, 580, 715, 1092, 1200, 1450,



and 1580 cm^{-1} relative content of nickel oxide (Fig. S4).

Fig. S6 XRD patterns of WO_{3-x} , WO_3 , and FTO films.

X-ray diffraction (XRD) analysis confirmed the phase of WO_{3-x} and WO_3 are both crystallinity state. Except for the typical peaks of FTO, the XRD spectra of WO_{3-x} and WO_3 show the diffraction peaks at angles $2\Theta=24.1^\circ$, 28.6° , 33.8° , 41.4° , 49.6° , and 55.6° , which associated with the monoclinic tungsten oxide. It also proves that using Coca-Cola and deionized water as solution to prepare electrochromic thin films has no effect on tungsten oxide crystal structure by the same prepared processing.

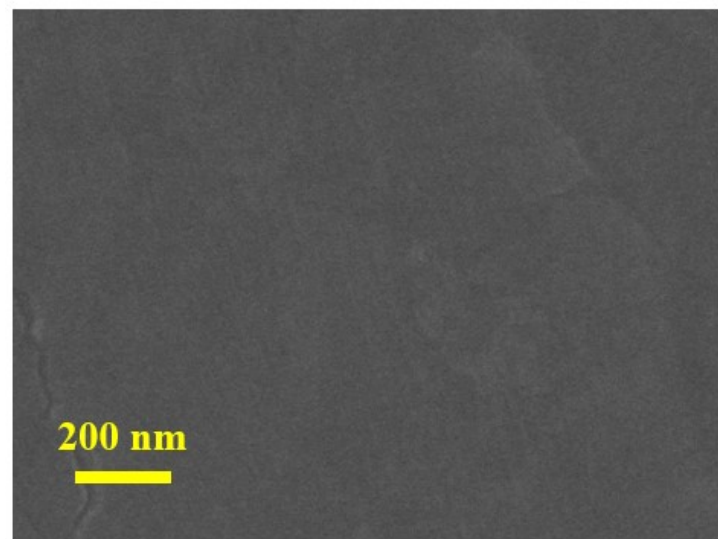


Fig.S7 SEM image of annealed WO_3 film

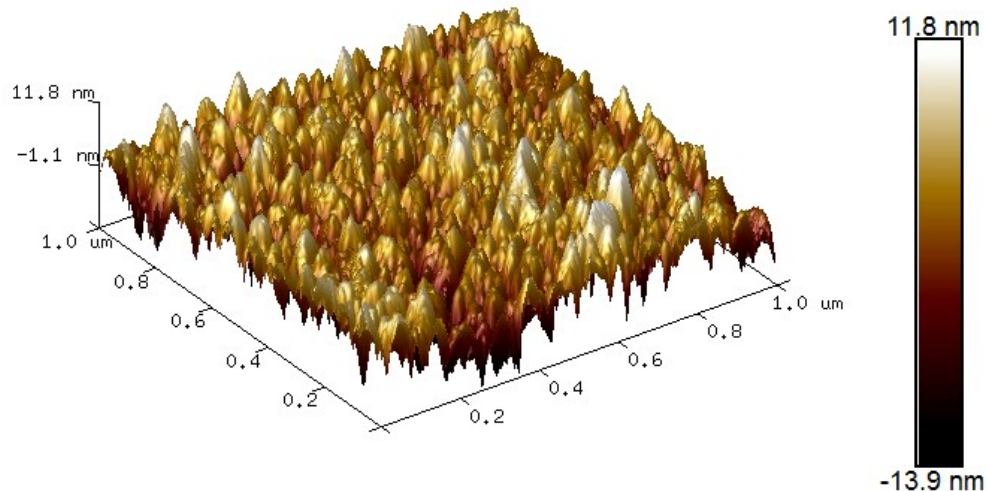


Fig. S8 AFM image of the WO_{3-x} film.

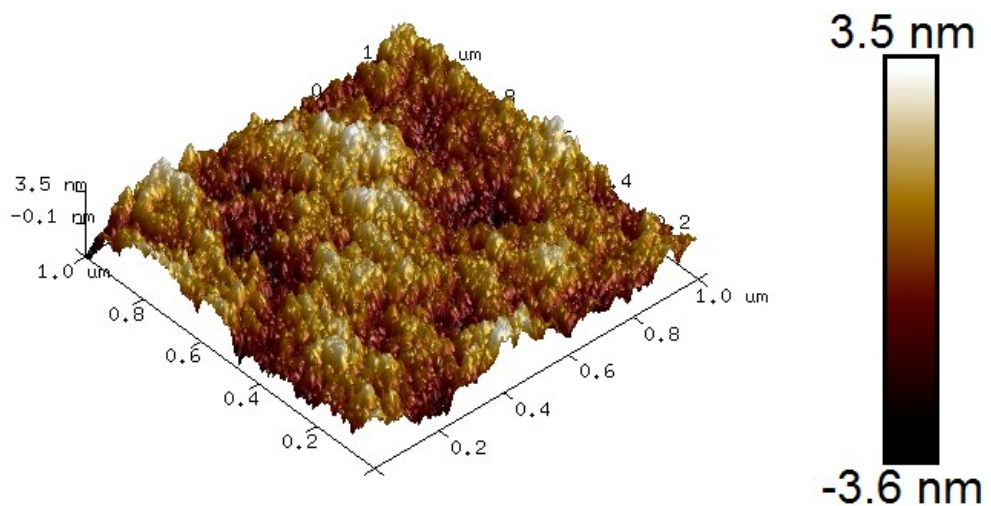


Fig. S9 AFM image of the WO_3 film.

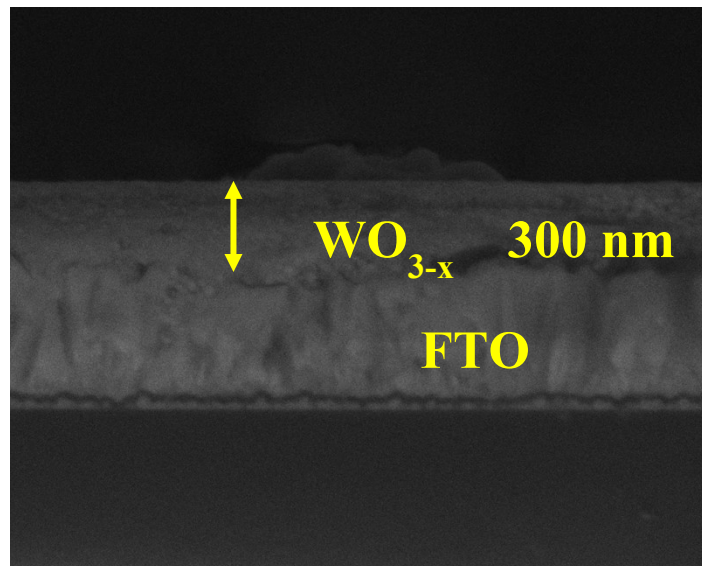


Fig. S10 The cross-sectional SEM image of WO_{3-x} film.

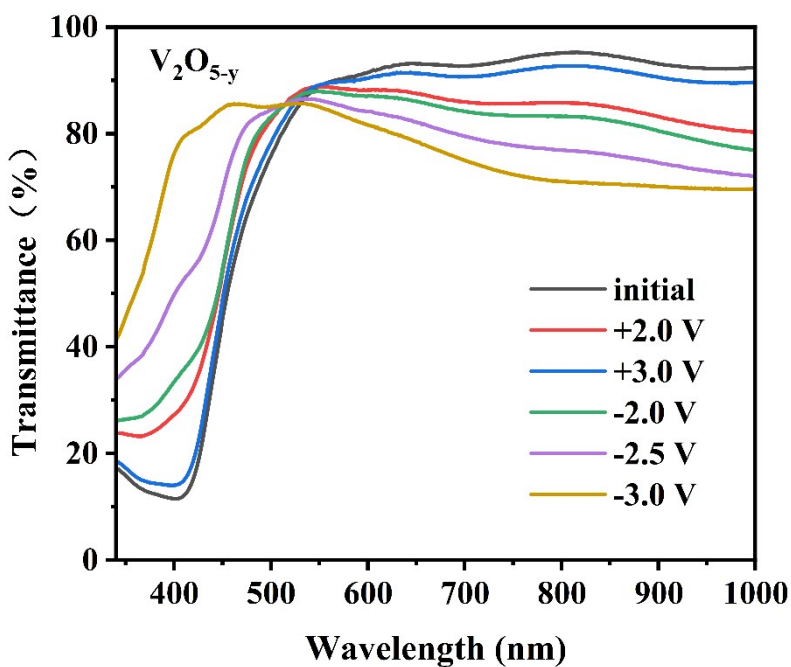


Fig. S11 Transmittance spectra of the vanadium pentoxide thin film at colored and bleached state.

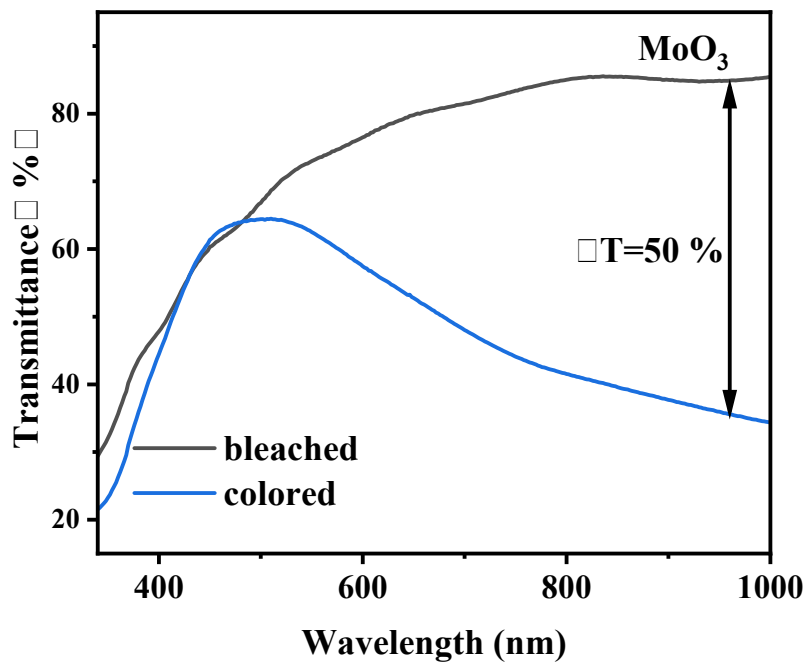


Fig. S12 Transmittance spectra of the molybdenum oxide thin film at colored and bleached state.

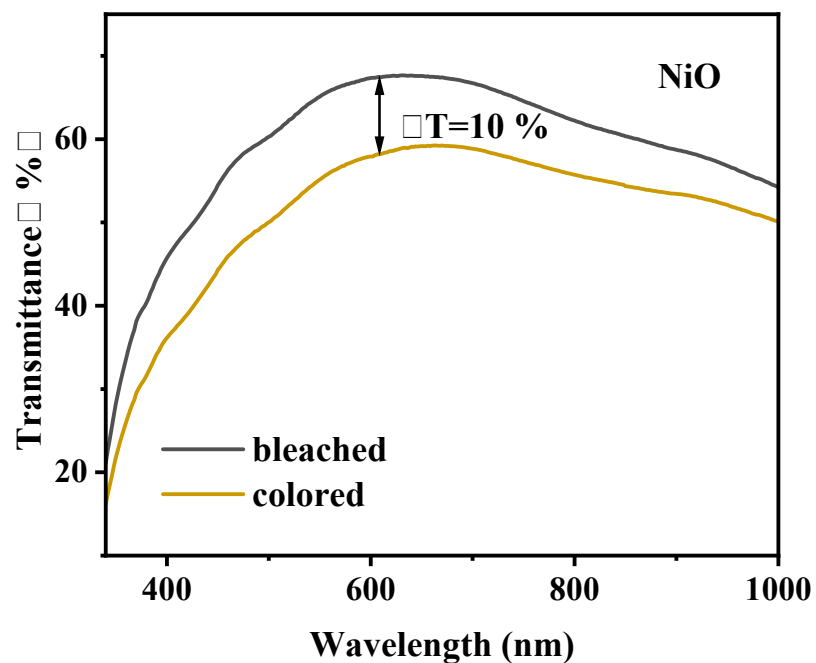


Fig. S13 Transmittance spectra of the nickel oxide thin film at colored and bleached state.

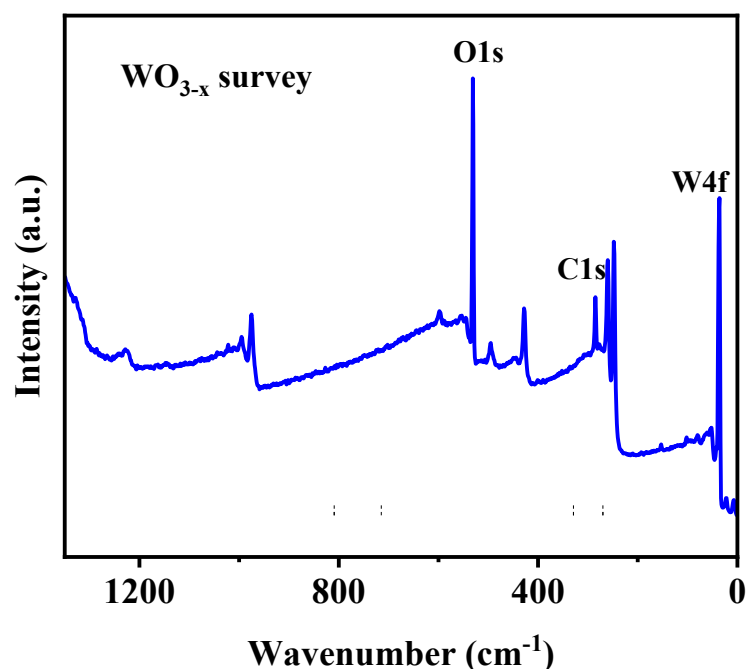


Fig. S14 XPS spectra of the self-doped WO_{3-x} film.

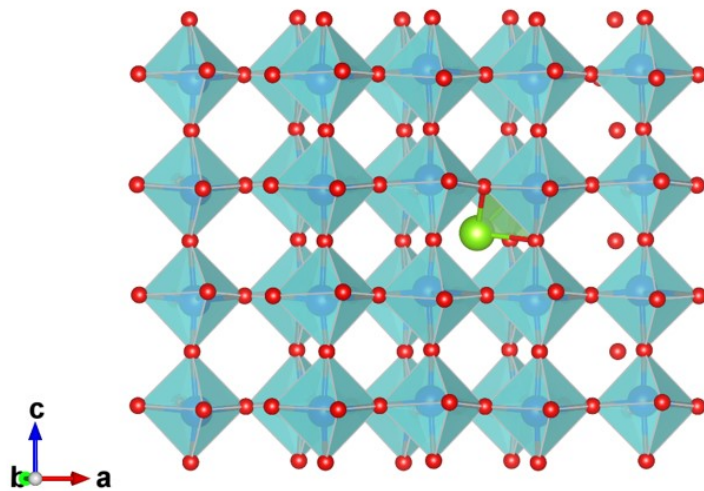


Fig. S15 The model of Li^+ insertion in pure WO_3 .

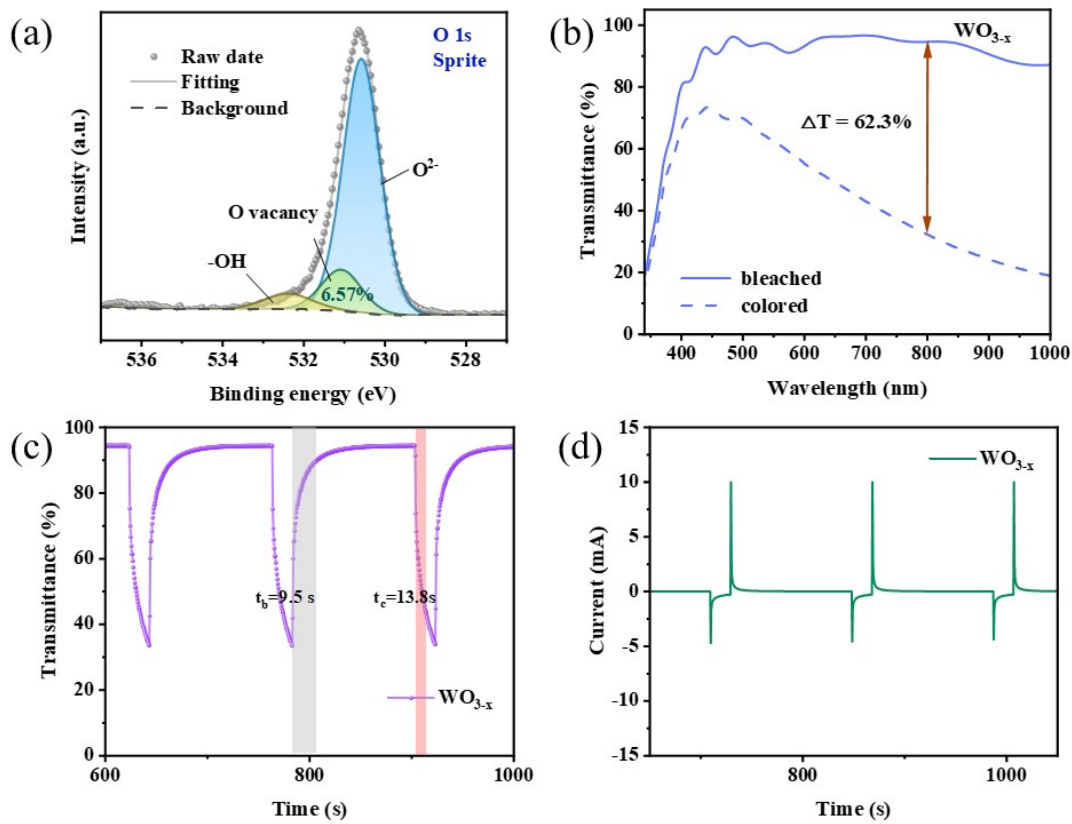


Fig. S16 a) O1s XPS spectrum of the annealed WO_{3-x} films (Sprite). b) Transmittance spectra of the self-doped WO_{3-x} thin film (Sprite) at colored and bleached states. c)

The switching behavior of the WO_{3-x} thin film (Sprite) at 800 nm. d) The chronoamperometry curve of WO_{3-x} thin film (Sprite) during the switching test.

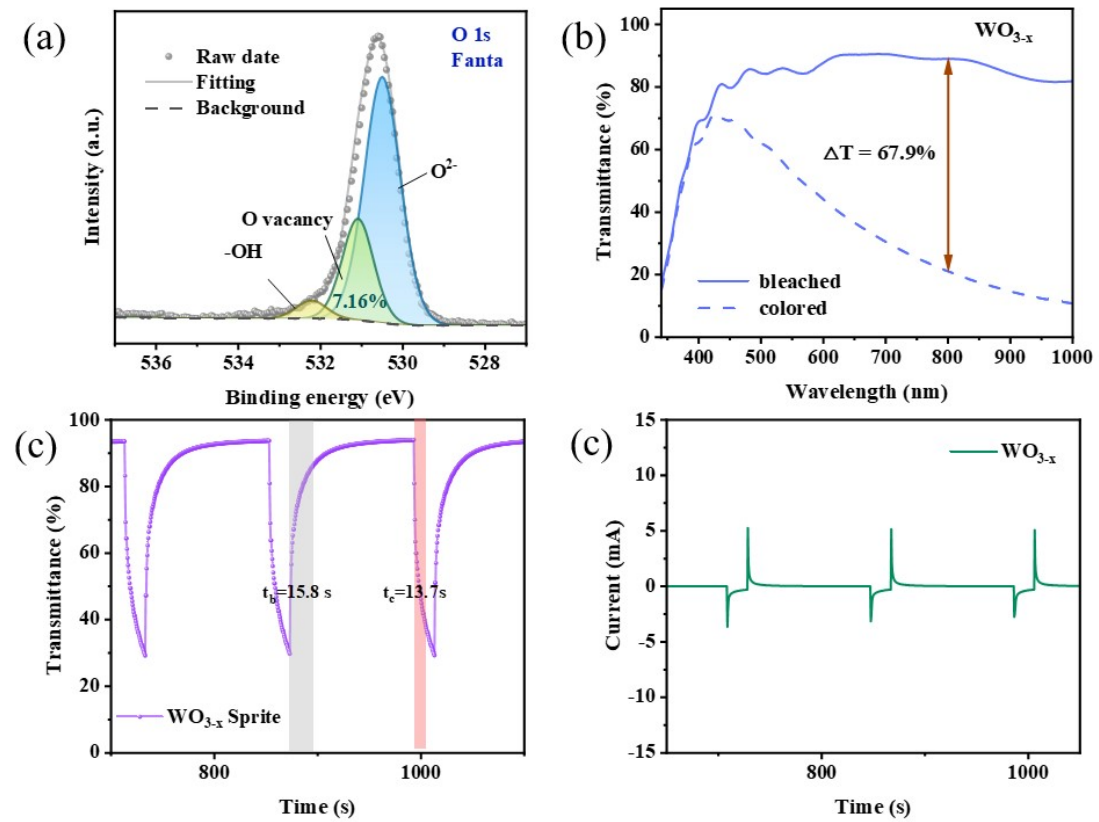


Fig. S17 a) O1s XPS spectrum of the annealed WO_{3-x} films (Fanta). b) Transmittance spectra of the self-doped WO_{3-x} thin film (Fanta) at colored and bleached states. c) The switching behavior of the WO_{3-x} thin film (Fanta) at 800 nm. d) The chronoamperometry curve of WO_{3-x} thin film (Fanta) during the switching test.

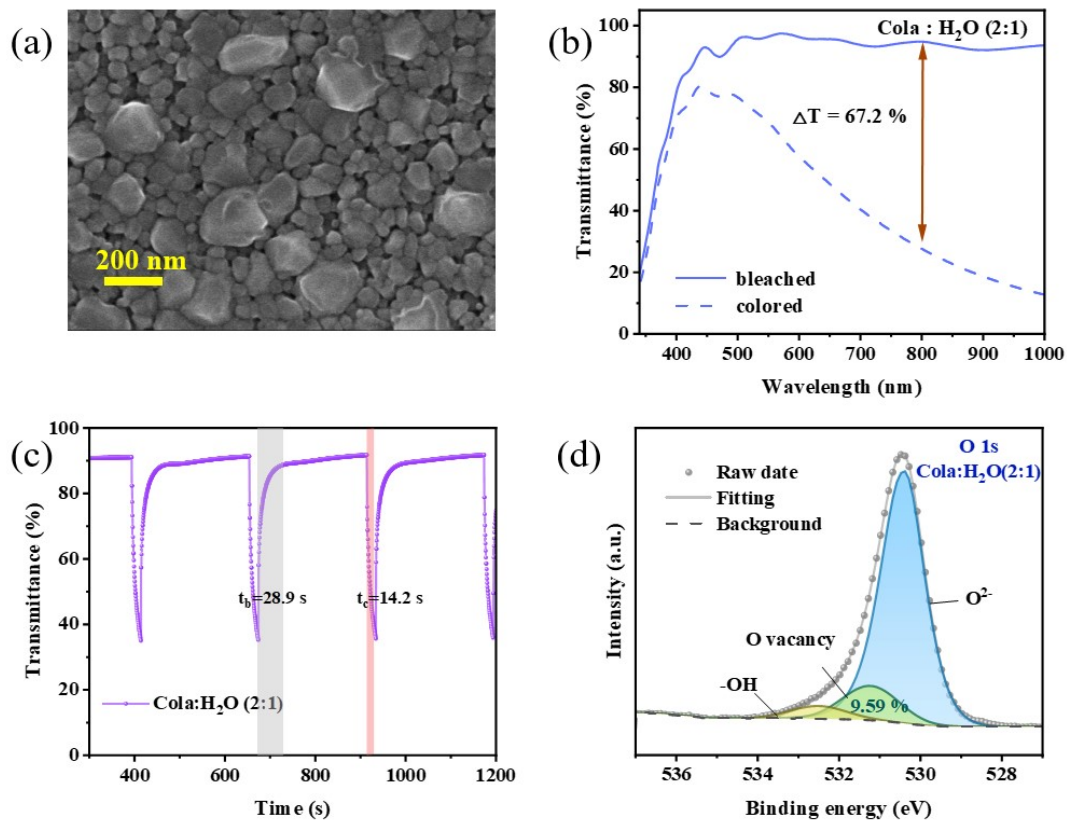


Fig. S18 Characterization of the morphology and properties of annealed self-doped $\text{WO}_{3-\text{x}}$ film thin films ($\text{Cola} : \text{H}_2\text{O} = 2:1$): a) SEM image. b) Transmittance spectra. c) The switching behavior at 800 nm. d) O1s XPS spectrum.

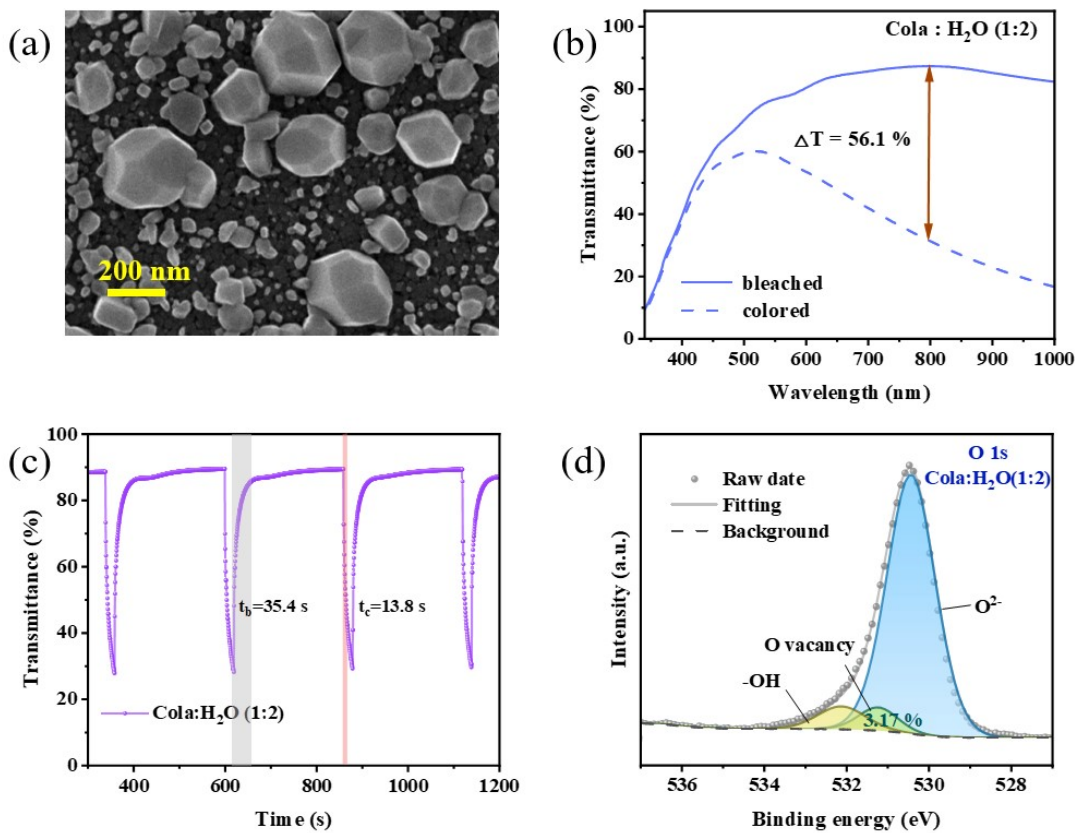


Fig. S19 Characterization of the morphology and properties of annealed self-doped $\text{WO}_{3-\text{x}}$ film thin films ($\text{Cola} : \text{H}_2\text{O} = 1:2$): a) SEM image. b) Transmittance spectra. c) The switching behavior at 800 nm. d) O1s XPS spectrum.

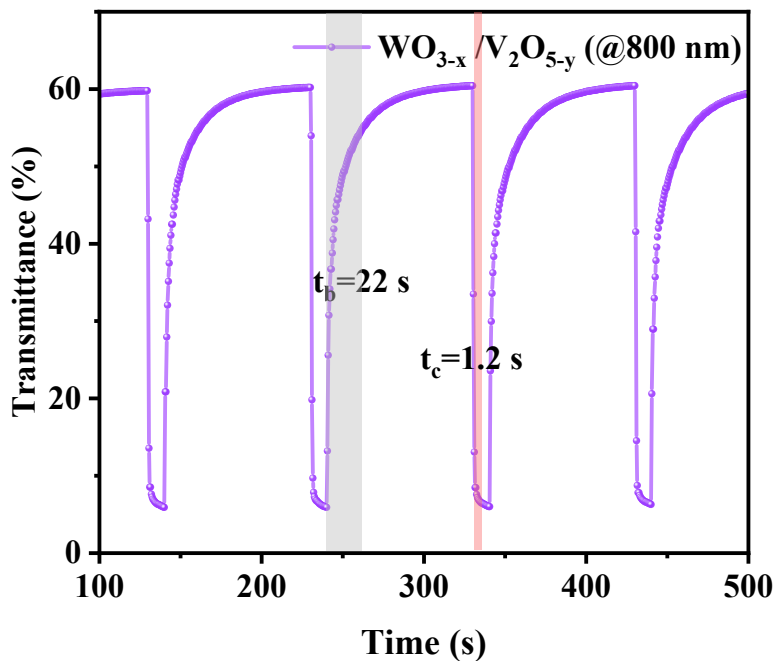


Fig. S20 The switching behavior of $\text{WO}_{3-\text{x}}/\text{V}_2\text{O}_{5-\text{y}}$ electrochromic device at 680 nm.

Table S1 Performance summary of the tungsten oxide based electrochromic materials

Materials	Fabrication method	ΔT (%)	CE (c m ² C ⁻¹)	tb(s)	tc(s)	D (cm ² s ⁻¹)	references
$\text{WO}_{3-\text{x}}$	carbonated beverages solution method	81.2@800 nm	98.7	23.0	11.5	1.1×10^{-10} (Li ⁺)	This work
WO_3 nanosheets	solution-phase synthesis	62.57@700 nm	-	6.97	10.74	1.01×10^{-9} (Li ⁺)	1
coral-like nanostructure WO_3	hydrothermal synthesis	78.1@630 nm	56.5	6.0	5.0	-	2
WO_3 quantum-dots	solution-based deposition	97.8@633 nm	76.8	4.5	4.0	5.59×10^{-9} (Li ⁺)	3
Tb-doped WO_3	hydrothermal synthesis	66.71@680 nm	48.33	3.70	9.99	-	4
Ti-doped WO_3	wet bath	67.6@633 nm	106.6	5	15	4.42×10^{-9} (H ⁺)	5
WO_3 nanotree-like structures	solvothermal	74.7@630	75.35	2.64	7.28	-	6

			nm						
WO ₃	magnetron sputtering	72.5@1000 nm 93.9@633 nm	80.5	3.0	5.3	9.8×10 ⁻¹⁰ (Li ⁺)			7
WO ₃	eletrodeposition and magnetron	nm ; 89.6@1500 nm	92.3	3.6	3.0	-			8
hexagonal/amorphous tungsten oxide core/shell nanorod arrays	hydrothermal treatment and spin coating	67.7@800 nm	101	21	15	8.08×10 ⁻¹⁰ (H ⁺)			9
P-doped WO ₃	ignition reaction	55.8@633 nm	55.9	2.5	6.1	7.21×10 ⁻⁹ (Li ⁺)			10
WO ₃ @AgNW core-shell nanowire	hydrothermal synthesis	72@550 nm	78.64	8	11	-			11
WO ₃ /PEDOT core/shell hybrid nanorod arrays	solvothermal and in situ electropolymerization	72@633 nm	163.5	3.6	3.8	-			12
WO ₃ nanoparticle	sol-gel method and inkjet-printed	75.4@633 nm	131.9	13.1	10	-			13
P ₈ W ₄₈ / W ₁₈ O ₄₉ Nanowires	layer-by-layer self-assembly	61.4@1060 nm	121.03	78	86	-			14
Porous a-WO ₃ /Ag NFs/WO ₃	magnetron sputtering and electrospinning	89.7@633 nm	58.95	19	9	-			15
MoO _{3-y} /WO _{3-x}	ball-milling and spin-coating	50@660 nm	-	15	4	2.13×10 ⁻¹³ (Al ³⁺)			16
WO ₃	reactive sputtering	74.4@670 nm	76.45	2.2	7.7	-			17
WO _{3-x}	spin-coating	70@680 nm	62	15	7	1.0×10 ⁻¹⁰ (Li ⁺)			18

References

- 1 A. Azam, J. Kim, J. Park, T. G. Novak, A. P. Tiwari, S. H. Song, B. Kim and S. Jeon, *Nano Lett.*, 2018, **18**, 5646-5651.
- 2 J. B. Pan, Y. Wang, R. Z. Zheng, M. T. Wang, Z. Q. Wan, C. Y. Jia, X. L. Weng, J. L. Xie and L. J. Deng, *J. Mater. Chem. A*, 2019, **7**, 13956-13967.
- 3 Y. J. Yao, Q. Zhao, W. Wei, Z. Chen, Y. Zhu, P. Zhang, Z. T. Zhang and Y. F. Gao, *Nano Energy*, 2020, **68**, 104350.
- 4 L. Y. Shen, J. M. Zheng and C. Y. Xu, *Nanoscale*, 2019, **11**, 23049-23057.
- 5 Y. Zhan, M. R. J. Tan, X. Cheng, W. M. A. Tan, G. F. Cai, J. W. Chen, V. Kumar, S. Magdassi and P. S. Lee, *J. Mater. Chem. C*, 2017, **5**, 9995-10000.
- 6 Y. Q. Li, W. A. McMaster, H. Wei, D. H. Chen and R. A. Caruso, *ACS Appl. Nano Mater.*, 2018, **1**, 2552-2558.
- 7 Y. Zhao, X. Zhang, X. Chen, W. Li, L. Wang, F. Ren, J. Zhao, F. Endres and Y. Li,

- ACS Sustain. Chem. Eng.*, 2020, **8**, 11658-11666.
- 8 Y. D. Shi, M. J. Sun, Y. Zhang, J. W. Cui, Y. Wang, X. Shu, Y. Q. Qin, H. H. Tan, J. Q. Liu and Y. C. Wu, *Sol. Energ. Mat. Sol. C.*, 2020, **212**, 110579.
 - 9 X. T. Huo, H. Y. Zhang, W. G. Shen, X. W. Miao, M. Zhang and M. Guo, *J. Mater. Chem. A*, 2019, **7**, 16867-16875.
 - 10 K. Bon-Ryul, K. H. Kim and H. J. Ahn, *Nanoscale*, 2019, **11**, 3318-3325.
 - 11 T. T. Hao, S. Wang, H. B. Xu, X. Zhang, J. Y. Xue, S. K. Liu, Y. Song, Y. Li and J. P. Zhao, *Chem. Eng. J.*, 2021, **426**, 130840.
 - 12 Y. D. Shi, Y. Zhang, K. Tang, J. W. Cui, X. Shu, Y. Wang, J. Q. Liu, Y. Jiang, H. H. Tan and Y. C. Wu, *Chem. Eng. J.*, 2019, **355**, 942-951.
 - 13 G. F. Cai, P. Darmawan, M. Q. Cui, J. W. Chen, X. Wang, A. L. S. Eh, S. Magdassi and P. S. Lee, *Nanoscale*, 2016, **8**, 348-357.
 - 14 H. X. Gu, C. S. Guo, S. H. Zhang, L. H. Bi, T. C. Li, T. D. Sun and S. Q. Liu, *ACS Nano*, 2018, **12**, 559-567.
 - 15 Y. A. Wang, Z. H. Meng, H. Chen, T. Li, D. J. Zheng, Q. C. Xu, H. Wang, X. Y. Liu and W. X. Guo, *J. Mater. Chem. C*, 2019, **7**, 1966-1973.
 - 16 W. T. Wu, H. J. Fang, H. L. Ma, L. L. Wu, Q. Wang and H. Wang, *ACS Appl. Mater. Interfaces*, 2021, **13**, 20326-20335.
 - 17 L. L. Xie, S. W. Zhao, Y. Zhu, Q. X. Zhang, T. C. Chang, A. B. Huang, P. Jin, S. Ren and S. H. Bao, *ACS Sustain. Chem. Eng.*, 2019, **7**, 17390-+.
 - 18 L. J. Zhou, P. Wei, H. J. Fang, W. T. Wu, L. L. Wu and H. Wang, *J. Mater. Chem. C*, 2020, **8**, 13999-14006.